fluids

MDPI

Article

Efficiency Improvement of Darrieus Wind Turbine Using Oscillating Gurney Flap

Alaeddine Zereg [1], Mounir Aksas [2], Mohamed Taher Bouzaher [3], Salah Laghrouche [4] and Nadhir Lebaal [5,*]

[1] LPEA, Department of Physics, University of Batna 1, Batna 05000, Algeria; alaeddine.zereg@univ-batna.dz
[2] Higher National School of Renewable Energy, Environment & Sustainable Development, Batna 05078, Algeria; mounir.aksas@hns-re2sd.dz
[3] Scientific and Technical Research Centre for Arid Areas (CRSTRA), Biskra 07000, Algeria; mohamedbouzaher2@gmail.com
[4] Energy Department, FEMTO-ST Institute (UMR 6174), UTBM, Université Bourgogne Franche-Comté, CNRS, 90010 Belfort, France; salah.laghrouche@utbm.fr
[5] ICB-COMM, University of Technology Belfort-Montbéliard, 90010 Belfort, France
* Correspondence: nadhir.lebaal@utbm.fr

Abstract: In this work, a new model of Darrieus wind turbines with an oscillating gurney flap (OGF) is proposed. A detailed 2D computational fluid dynamics (CFD) investigation is carried out using ANSYS-Fluent 22.0 to assess the turbine performance. The OGF can alter its position between the upper and lower blade surfaces during the turbine rotation. Equations related to the combined motion are implemented through a user-defined function (UDF). The proposed model is validated where a good coincidence is achieved. The overset dynamic mesh method is used. It was found that a judicious synchronization of OGF and turbine blades creates beneficial vortex interactions, which correct the pressure distribution and lead to an overall improvement in the lift force. The magnitude of the improvement is highly dependent on the OGF length and the phase motion φ. The average torque coefficient Cm for the controlled case increased by more than 19% in comparison with the nominal case.

Keywords: Darrieus wind turbines; oscillating gurney flap; performance enhancement; CFD

check for updates

Citation: Zereg, A.; Aksas, M.; Bouzaher, M.T.; Laghrouche, S.; Lebaal, N. Efficiency Improvement of Darrieus Wind Turbine Using Oscillating Gurney Flap. *Fluids* **2024**, *9*, 150. https://doi.org/10.3390/fluids9070150

Academic Editor: Tim Persoons

Received: 3 May 2024
Revised: 14 June 2024
Accepted: 17 June 2024
Published: 22 June 2024

Copyright: © 2024 by the authors. Licensee MDPI, Basel, Switzerland. This article is an open access article distributed under the terms and conditions of the Creative Commons Attribution (CC BY) license (https://creativecommons.org/licenses/by/4.0/).

1. Introduction

The use of renewable energy sources such as wind energy has become increasingly important in recent years. It can be considered as an efficient solution to reduce the dependence on fossil fuels and mitigate their impact on climate change. Among different types of wind turbines, vertical axis wind turbines (VAWTs) have gained attention in recent years as a promising technology for small-scale and distributed wind energy systems [1–3]. VAWTs do not require a yaw mechanism to align with the wind direction, which makes them more suitable for urban and low-wind-speed environments. However, the performance of VAWTs is still not comparable with that of horizontal axis wind turbines (HAWTs) [4], mainly due to the complex flow dynamics around the turbine blades. Among potential solutions to improve the performance of VAWTs is the use of a gurney flap, which is a small flap attached to the trailing edge of the turbine blade [5,6]. The gurney flap (GF) has attracted significant interest among researchers as a passive flow control device. This is primarily because of its simple geometry modification, low production cost, and notable performance enhancement, particularly at low tip speed ratios (TSRs). Recently, an innovative GF concept has been proposed by several researchers, which is the oscillating or deformable gurney flap OGF. The OGF can alter its position between the upper and lower blade surfaces during the turbine flapping or rotation [7,8].

The oscillating gurney flap corrects the pressure distribution on the surface of the blade, which increases the lift and reduces the drag on the blade. This increases the turbine's

efficiency and, thus, the output power [9]. The oscillation of the flap can be performed actively using a small motor, or passively by the wind load.

The effects of using gurney flaps (GFs) are highly dependent on their configuration, including their geometric features and mounting details [10,11]. Among these factors, the GF height plays a crucial role as a pivotal parameter. Increasing the height of the flap enhances lift forces [12]. However, it also increases the drag force, and if the flap height exceeds a certain value, the magnitude of the drag force can delay the benefits of using GFs [13,14]. Therefore, finding the optimal flap height is important to strike a balance between lift enhancement and drag reduction [15].

Liebeck [16] conducted the initial experimental modification on a Newman airfoil by incorporating a vertical gurney flap (GF) to enhance the lift coefficient. Their results show that when the height of the vertical GF is up to 1.25% of the airfoil chord length (c), there is a significant increase in lift with only a slight increase in drag force. However, when the GF height exceeds 2% of the chord length, the drag coefficient increases rapidly. The presence of GF leads to the generation of alternating shed vortices in the downstream wake. In an experimental study conducted by Gerontakos and Lee [17], the dynamic stall characteristics of a NACA 0012 airfoil were investigated using gurney flaps of 1.6% and 3.2% chord height. The findings indicated that the dynamic stall angle can be altered by controlling the mounting angle of the gurney flaps. Giguère et al. [18] numerically demonstrated that gurney flaps with a height ranging from 0.5% to 5% of the chord length efficiently increased the lift force while causing only a minimal increase in drag forces. The optimal flap height was found to be equal to the boundary layer thickness at the trailing edge. In their study, Pastrikakis et al. [19] proved that adding a gurney flap had a notable impact on the flow field and pressure distribution around the blade, leading to improved blade performance. Additionally, Bianchini et al. [20] demonstrated that the gurney flap can enhance the self-starting capability of Vertical Axis Wind Turbines. This improvement allows the turbine to initiate rotation at very low incoming wind speeds or within a low range of tip speed ratios (TSRs), thus reducing the reliance on external power sources. Xiao et al. [21] have performed a numerical simulation to examine the effects of pitching trailing edge flaps on a vertical axis tidal turbine (VATT). The findings revealed a significant enhancement of 28% in the power coefficient of the turbine compared to a traditional blade turbine. In a separate study, Feng [22] developed a virtual gurney flap using a dielectric barrier discharge plasma actuator. The research demonstrated that this novel device effectively improved the lift coefficient. In their work, T. Syawitri [23] demonstrated that the inclusion of gurney flaps (GFs) in VAWT blades effectively delays deep stalls, resulting in the elimination of a negative instantaneous moment coefficient and an overall enhancement in turbine performance. Ismail et al. [24] examined the performance of an oscillating blade with a GF mounted on a NACA0015 airfoil. Their findings revealed a 35% increase in the average tangential force under steady-state conditions and a 40% increase under oscillating conditions (over one period).

Chen et al. [25] implemented fixed gurney flaps (GFs) on the outer side of each wind turbine blade. However, this configuration resulted in a net decrease in the power coefficient compared to the original design of the turbine. It was concluded that the fixed GFs did not effectively adapt to the varying angles of attack during VAWT operation. In a separate study, Mayda et al. [26] investigated VAWT performance and highlighted that the installation of GFs exclusively on the pressure side of the airfoil improved its aerodynamic performance.

Bouzaher et al. [27], added a gurney flap to the trailing edge of a flapping turbine at Re = 1100. When the motion of the GF synchronized with the flapping motion, a virtual camber was generated, which helped to improve the output power. Furthermore, the control of the leading-edge vortex development was found to further enhance the lift production.

Previous research discussed gurney flaps that were either permanent or adjustable but did not take into account the effect of their motion. The main objective of this work

is to systematically assess the effect of a new type of gurney flap on the flow structure and aerodynamics performances around a VAWT, and to compute the energy extraction improvement introduced by the new gurney flap. In a word, the purpose of our study is to extend the gurney flap's application in energy fields. The mechanism of flow control is investigated and the length of the movable GF and its motion phase is carried out. The model is validated against experimental results available in the literature.

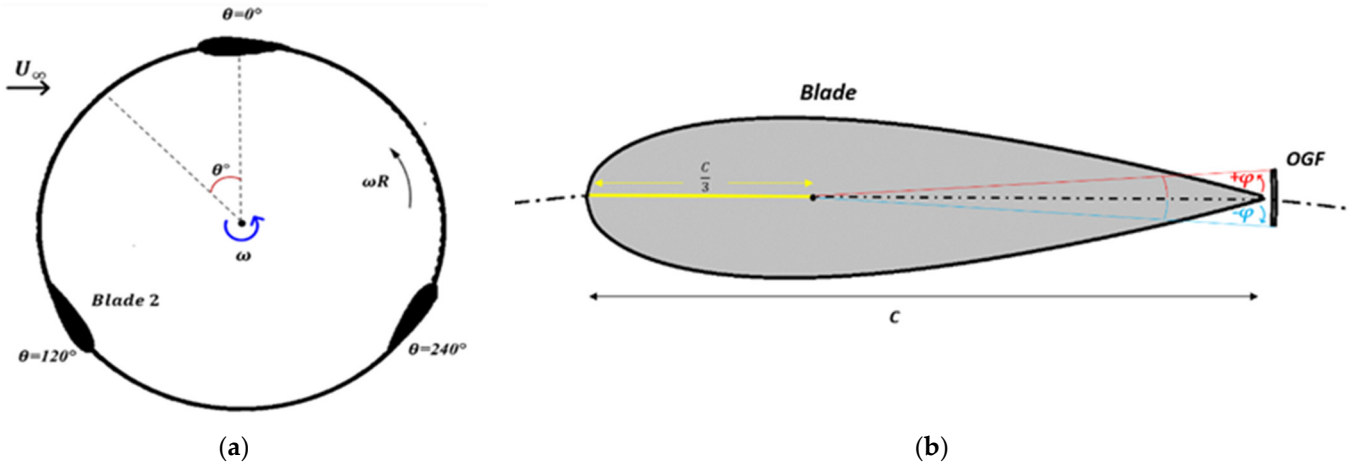
This study aims to provide a better understanding of the potential benefits of using an oscillating gurney flap in VAWTs and to guide the design of more efficient VAWTs.

2. Turbine Geometrical Parameters

Table 1 shows the geometric parameters of a three-blade Vertical Axis Wind Turbine (VAWT) rotor examined in this study. Previous work has used the same rotor design for 2D simulations [25]. Since 3D simulations are computationally expensive, we opted for a 2D computational domain (Figure 1). Although connecting rods could have a significant impact, a study by Rezaeiha et al. [28] showed that even with a shaft–diameter ratio of 16%, the maximum power only experienced a minor 5.5% decrease compared to a VAWT without shaft interference. Therefore, the shaft and connecting rods are disregarded. Our primary objective was to investigate the effect of OGF (presumably referring to a specific feature or modification) on VAWT performance, including wake interaction and flow curvature effects. Hence, the focus is put on these aspects, leading to the exclusion of the shaft and connecting rods from the study.

Table 1. Geometrical turbine parameters.

Diameter (D) [mm]	1030
Chord (C) [mm]	85.5
Blade profile	NACA0021
Number of blades	3
Solidity (σ)	0.5
Spoke–blade connection	0.33
Gurney flap pitching center	0.33c



(**a**) (**b**)

Figure 1. Schematic diagram of the turbine (**a**) and OGF–blade (**b**) model.

3. Numerical Method and Turbulence Model

3.1. Governing Equations

In the current simulation, the Unsteady Reynolds-averaged Navier–Stokes equations (URANS) (Equations (1) and (2)) are solved using the ANSYS-FLUENT 22.R1 software

package. These equations govern the behavior of a transient incompressible flow and involve the conservation of mass and momentum:

$$\nabla \cdot \vec{v} = 0 \tag{1}$$

$$\rho \frac{\partial \vec{v}}{\partial t} = \vec{F} - \nabla \cdot p + \mu \nabla^2 \vec{v} \tag{2}$$

where $\vec{v}$ is the vector of velocity, ρ is the density of fluid, $\vec{F}$ is the body force on the fluid, $\boldsymbol{p}$ is the pressure, and $\boldsymbol{\mu}$ is the dynamic viscosity.

The simulation assumes a two-dimensional configuration in an isothermal fluid domain. The SIMPLE algorithm is adopted for the pressure–velocity coupling with a Rhie-chow as a flux-type option. Least squares cell-based schemes are used for the gradient of spatial discretization. A second-order scheme is used for pressure and a second-order upwind for momentum. To account for turbulence, multiple turbulence models are evaluated [29], and the findings demonstrate that the realizable *k*-ε turbulent model offers an acceptable level of accuracy for the current problem. To effectively capture the near-wall boundary layer while maintaining a reasonable number of mesh points, the enhanced wall treatment technique is employed in conjunction with the *k*-ε turbulent model (Equations (3) and (4)). The specific turbulent model is governed by the following pair of equations:

$$\frac{\partial}{\partial t}(\rho k) + \frac{\partial}{\partial x_j}(\rho k u_j) = \frac{\partial}{\partial x_j}\left[\left(\mu + \frac{\mu_t}{\sigma_k}\right)\frac{\partial k}{\partial x_j}\right] + G_k + G_b - \rho\epsilon - Y_M + S_k \tag{3}$$

$$\frac{\partial}{\partial t}(\rho \varepsilon) + \frac{\partial}{\partial x_j}(\rho \varepsilon u_j)^2 = \frac{\partial}{\partial x_j}\left[\left(\mu + \frac{\mu_t}{\sigma_\epsilon}\right)\frac{\partial \varepsilon}{\partial x_j}\right] + \rho C_1 S\varepsilon - \rho C_2 \frac{\varepsilon^2}{k + \sqrt{\nu\epsilon}} + C_{1\epsilon}\frac{\varepsilon}{k} C_{3\varepsilon} G_b + S_\varepsilon \tag{4}$$

where

$$C_{1\varepsilon} = max\left[0.43, \frac{\eta}{\eta + 5}\right];\ C_{2\varepsilon} = 1.90;\ \eta = S\frac{k}{\epsilon};\ S = \sqrt{2S_{ij}S_{ij}} \text{ and } \sigma_\varepsilon = 1.2;\ \sigma_k = 1.0$$

In these equations, k is the turbulent kinetic energy and ε is the dissipation rate of kinetic energy, G_k represents the generation of turbulence kinetic energy due to the mean velocity gradients, G_b is the generation of turbulence kinetic energy due to buoyancy, and Y_M represents the contribution of the fluctuating dilatation in compressible turbulence to the overall dissipation rate. C_2 and C_1 are constants. σ_k and σ_ε are the turbulent Prandtl numbers for k and e, respectively. S_k and S_ε are source terms.

3.2. Computational Domain and Motion Modeling:

To perform the current 2D simulation, an overset dynamic mesh technique is used: it is a technique that allows the computational zones to move rigidly relative to each other via an overset interface. So, instead of updating the mesh cells itself, as is the case when using a Remeshing technique, the zones that contains the turbine blade and the oscillating gurney flap (OGF) move rigidly, which maintains the initial mesh quality and ensures a very good computational accuracy even with dynamic mesh. All cells information (pressure, velocity, etc.) will be transmitted via the overset interface and the mesh of each zone is uploaded separately in fluent (Figure 2). So, it is essential to take into consideration that the mesh density of each part will fit well together and with the basal mesh.

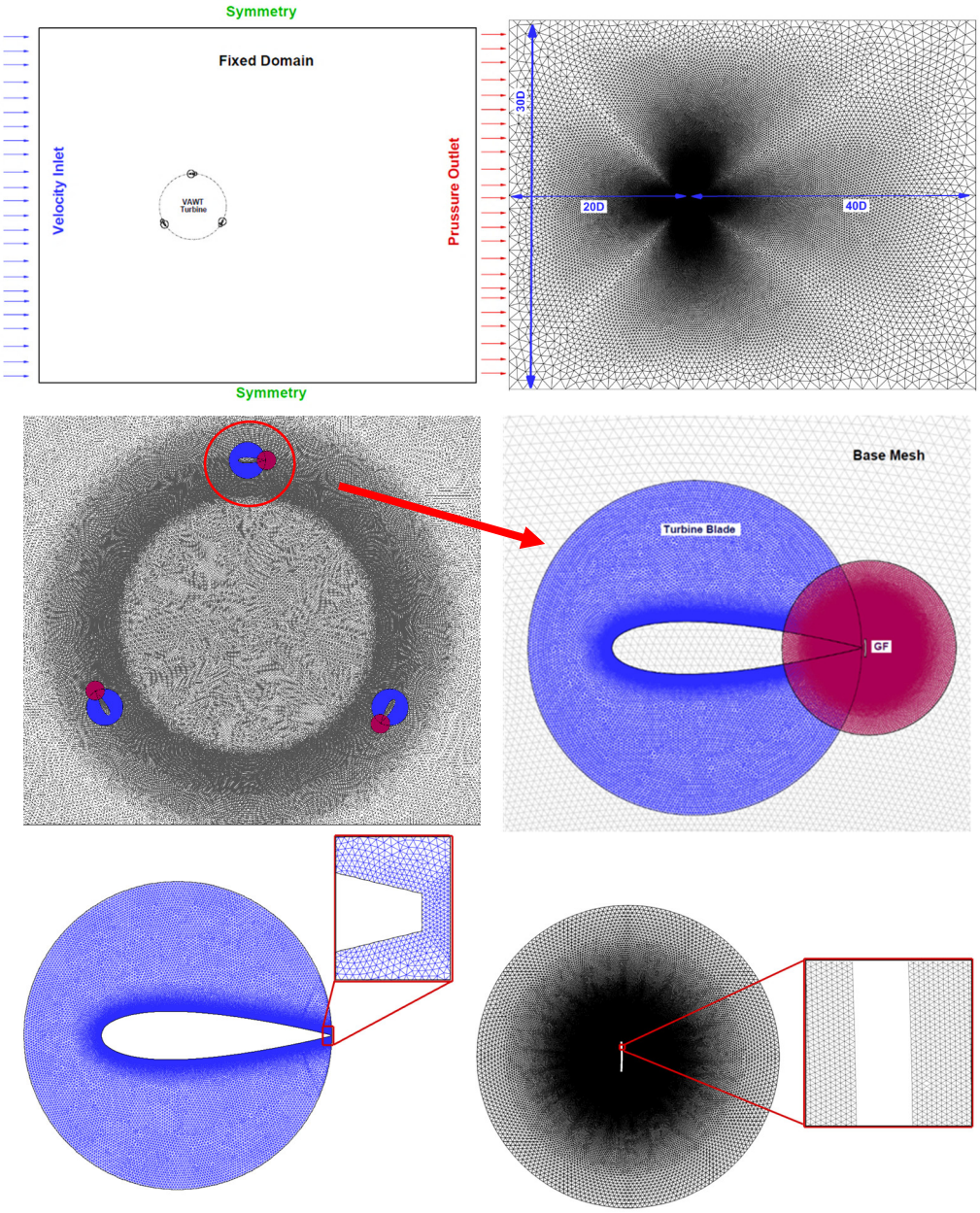


Figure 2. Computational domain and mesh distribution.

In order to investigate the dependence of the results on the computational grid, the simulation for the reference case is performed on three different grids: coarse, medium, and fine (see Table 2). As can be seen from Figure 3, good correlations between results are observed. A grid that has about 1,151,103 cells can precisely predict the moment coefficient and the fluid fields (Figure 3).

Table 2. Details of the computational meshes.

Mesh Size	Cells	Nodes	Number of Points on Blades	Maximum y+ on Blades
Coarse	602,905	301,455	1058	3.9
Medium	1,151,103	582,406	2054	2.82
Fine	2,014,430	1,013,386	3595	2.01

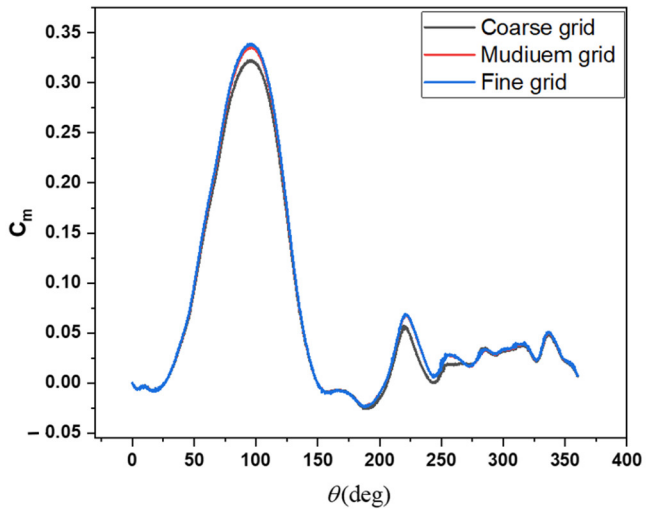


Figure 3. Instantaneous moment coefficients (grid-dependent test) for Blade 1.

Figure 4 shows that for Blade 3, the average value of y^+ is around unity, while the maximum local value is about 2.82.

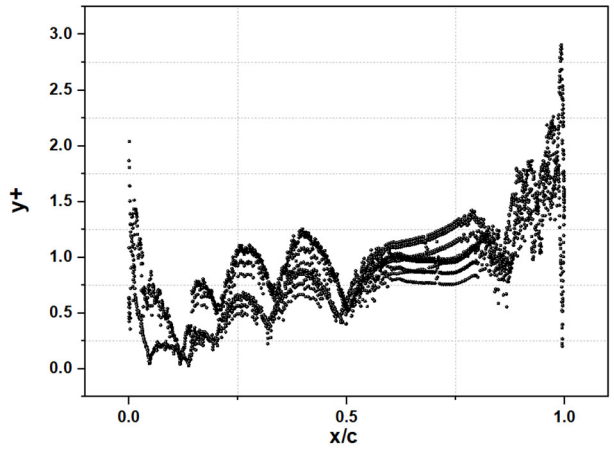


Figure 4. Variation of the dimensionless value y^+ along the cord length.

Regarding the user-defined function (UDF), the macro DEFINE_CG_MOTION is used. The movement equations (Equations (5)–(8)) of the OGF and the turbine blades are a combination of "Rotary transmission movement" and a pure rotation with respect to the center of the blade. They are given as follows:

$$x(t) = -R\ sin\ (2\pi ft) \tag{5}$$

$$y(t) = R\ cos\ (2\pi ft) \tag{6}$$

where R is the turbine radius, f is the pure rotation frequency, and t is the time.

- For the turbine blades:

$$\omega(t) = 2\pi f = cst \tag{7}$$

- For the GF:

$$\omega(t) = 2\pi f^* + A\ sin(2\pi f^* t + \varphi_n) \tag{8}$$

where A is the GF oscillation amplitude and f^* is the GF oscillation frequency. φ_n is the phase angle between rotation and oscillation and $n = 1, 2, 3$ represents an index for the blade number. Figure 5 displays the set Blade–OGF during the first quarter of the turbine cycle.

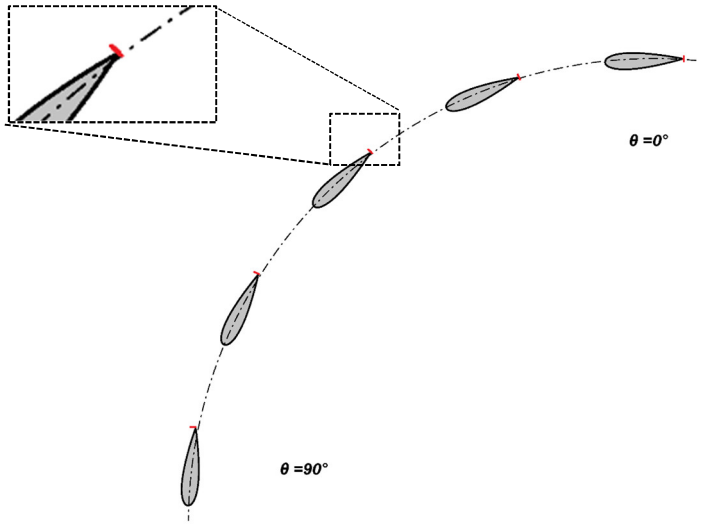


Figure 5. Blade with OGF (red) during the first quarter of the turbine cycle.

The current model has been validated against the work of Castelli et al. [30]. The calculated mean time power coefficient alongside the tip speed ratio, compared with the numerical results from Castelli et al. [30] is presented in Figure 6.

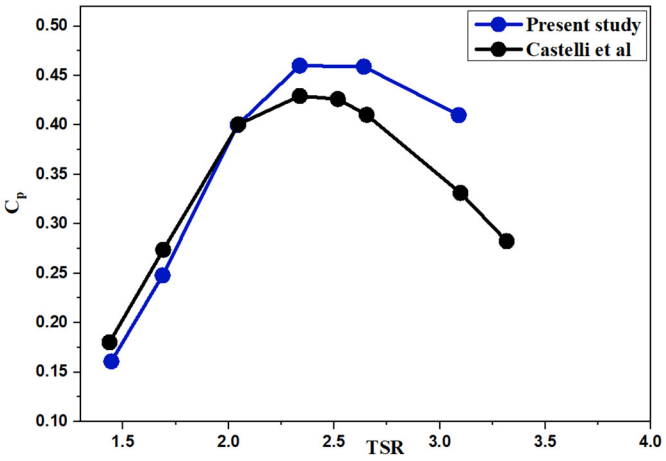


Figure 6. Time-averaged power coefficient against tip speed ratio (comparison with Castelli et al. [30]).

It is observed that the current power coefficient aligns with the results of Castelli et al. for a tip speed ratio of 2.04. However, some divergences appear for TSRs larger or less than 2.04. This could be attributed to the generation of strong flow separation at high-speed ratios. For TSRs less than 2.04, the discrepancy might stem from the different dynamic mesh techniques used in the two studies; specifically, Castelli et al.'s study employs a sliding mesh technique, whereas the current work utilizes an overset mesh technique.

The flow around a reversed D turbine (Wang et al. [31]) is also simulated as a second validation case. The main reason to select such case is that the turbine acts as a variable pitch turbine in the first half of the cycle. In addition, it involves the method of dynamic mesh (overset) and the pitching of flapping foil. The results of the time-varying drag coefficient for one period (Figure 7) indicate successful validation of the current solver against Wang et al.'s case, which will benefit this study.

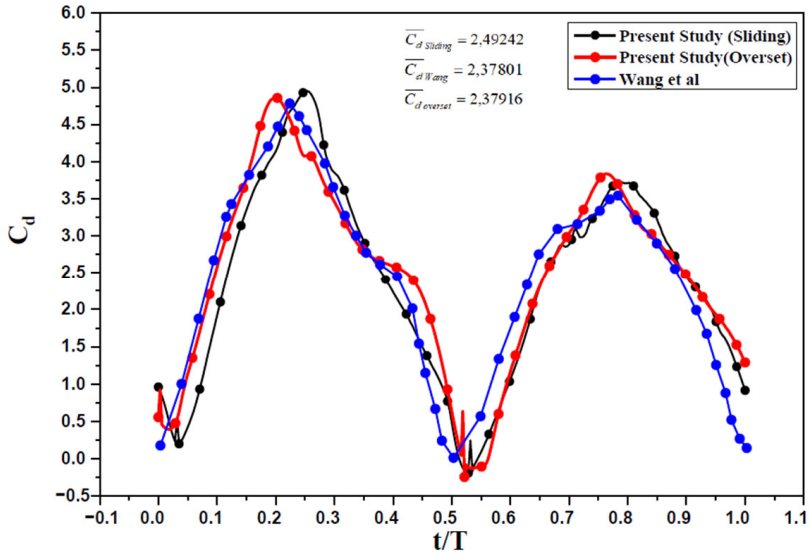


Figure 7. Time-varying drag coefficient for one period (comparison with Wang et al. [31]).

The reliability of the present solver is confirmed by testing it using three time steps. Figure 8 shows the results of the computational test. It can be observed that plots for two-time step sizes, 0.0005 s and 0.0001 s, overlap with each other. Consequently, the time-step test is validated. To minimize computational cost without sacrificing accuracy, the time step size of 0.0005 s is chosen.

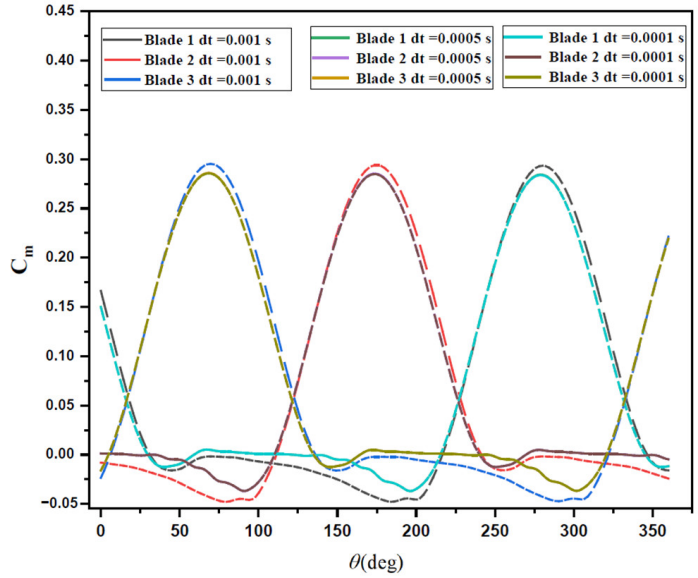


Figure 8. Individual time-varying torque coefficient versus time for one period.

The CFD simulations were carried out on a workstation, equipped with an Intel® Xeon® Gold 5218R CPU, 192 GB of the random-access memory (RAM), and NVIDIA Geo force RTX A6000 graphics card. The computational cost can be measured in units of time, like real universe time, or core time. Figure 9 illustrates the flowchart delineating the study process.

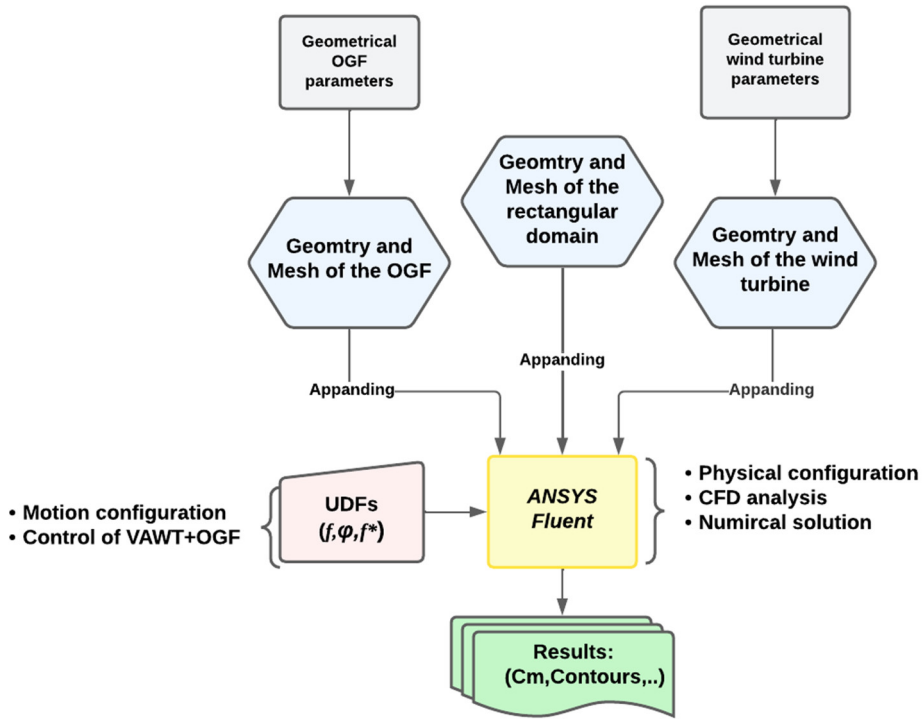


Figure 9. Flow chart of the study process.

4. Results and Discussion

4.1. Mechanism of Turbine Performance Improvement

To better understand the effect of oscillating gurney flap on the turbine output power, deeper analyses of the instantaneous torque coefficient for each blade during one turbine rotation as well as the pressure distribution along each blade are considered [32]. A comparative analysis between a simple blade turbine and a controlled case (with a gurney flap length L = (c/6, $\theta_1 = 3°$) is carried out.

Because the highest amount of energy is extracted in the first quarter of the turbine cycle ($0° < \theta < 90°$), the phase angle φ_n should be selected so that the OGF is fully located at the blade's upper-surface positive-pressure side in the first quarter of the turbine cycle for each blade. In this case, $\varphi_1 = 0°$, which means the swing motion of the OGF starts with blade 1 motion.

Figures 10 and 11 show the torque coefficient for three blades during one turbine cycle. It can be noted that with the presence of OGF, the total C_m peak increases from 0.2040 to 0.2269, which represents an improvement of about 11%. This is attributed to the fact that a fluid backflow is induced by OGF on the blade pressure side, which forces more the fluid to converge increasing the pressure on this blade side. On the contrary, the blade without OGF has a smooth fluid flow pattern near the trailing edge, which means there will be less backflow. The pressure contour displayed in Figure 12 shows that the presence of the gurney flap, at $\theta \simeq 45°$, gives rise to a high-pressure region near the blade's trailing edge.

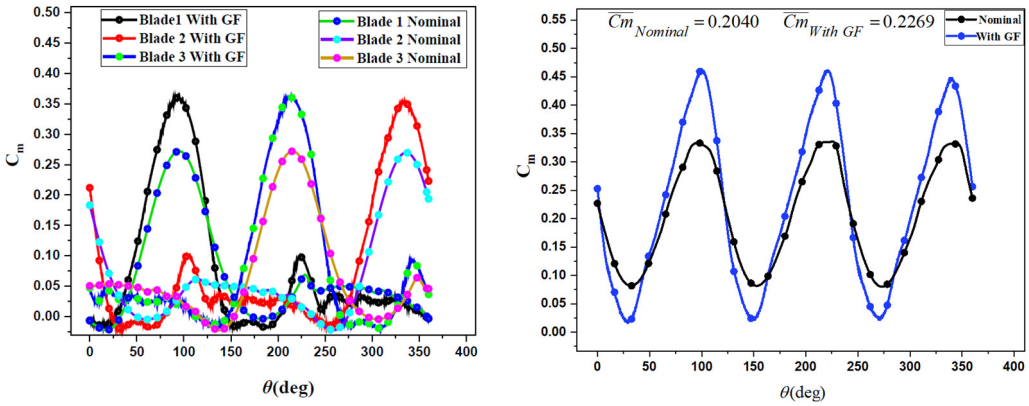


Figure 10. Comparison of instantaneous individual (**a**) and total torque (**b**) coefficient case: positive pressure side gurney flap.

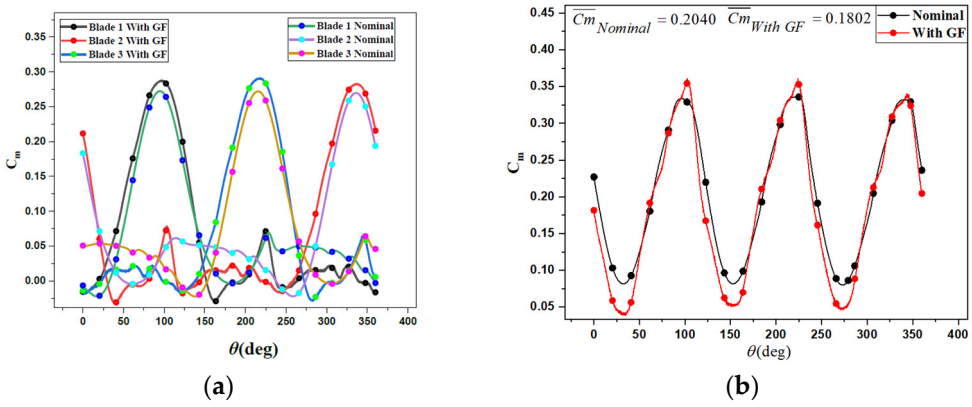


Figure 11. Comparison of instantaneous individual (**a**) and total torque (**b**) coefficient case: negative pressure side gurney flap.

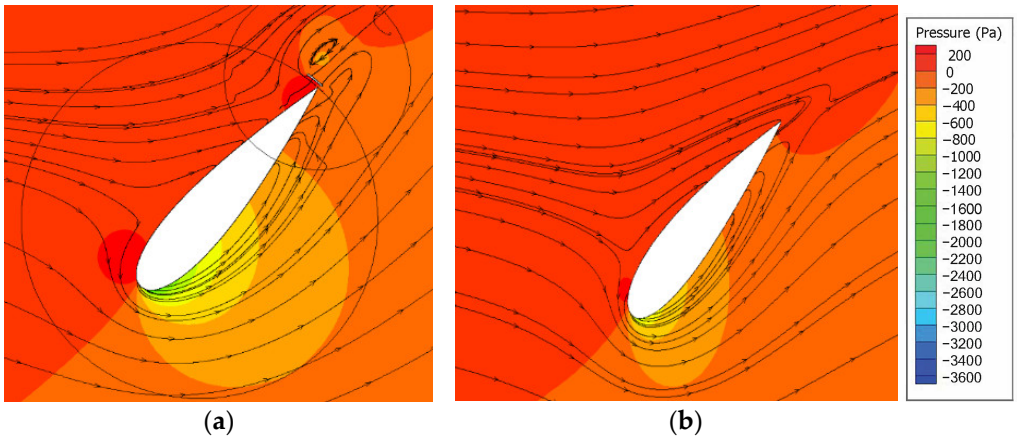


Figure 12. Comparison of pressure distribution for θ ≃ 45°: (**a**) with OGF, (**b**) nominal.

4.2. Effect of Motion Phase

The effect of the motion phase can be seen as the length of OGF, which positively affect the fluid backflow near the trailing edge. In other words, it indicates if the gurney flap is fully or partially located on the blade pressure side. Figure 13 represents how the phase motions are selected relative to the azimuthal angle. For a TSR = 2.04, five phase angles are tested.

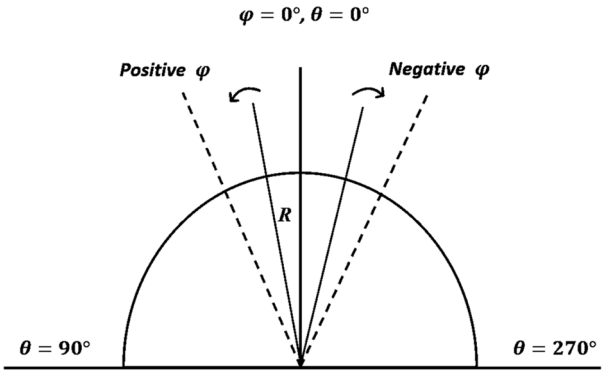


Figure 13. Selection of phase motions relative to azimuthal angle.

For various values of φ, it was noted that the phase angle that increases the GF length on the pressure side provides the highest peak of torque (Figure 14). For example, the selected negative phases make the gurney flap move toward the negative-pressure side by $9\pi/2$ and $-9\pi/2$ drying the cycle in the first quarter, which will negatively affect the torque and therefore the extracted power. The phase $\varphi = \pi/3$, makes the OGF act like a fixed GF, which generates two vortices near the trailing edge (Figure 15). The detachment of these vortices causes a fluctuation before the torque beak, which does not improve the efficiency of energy collection.

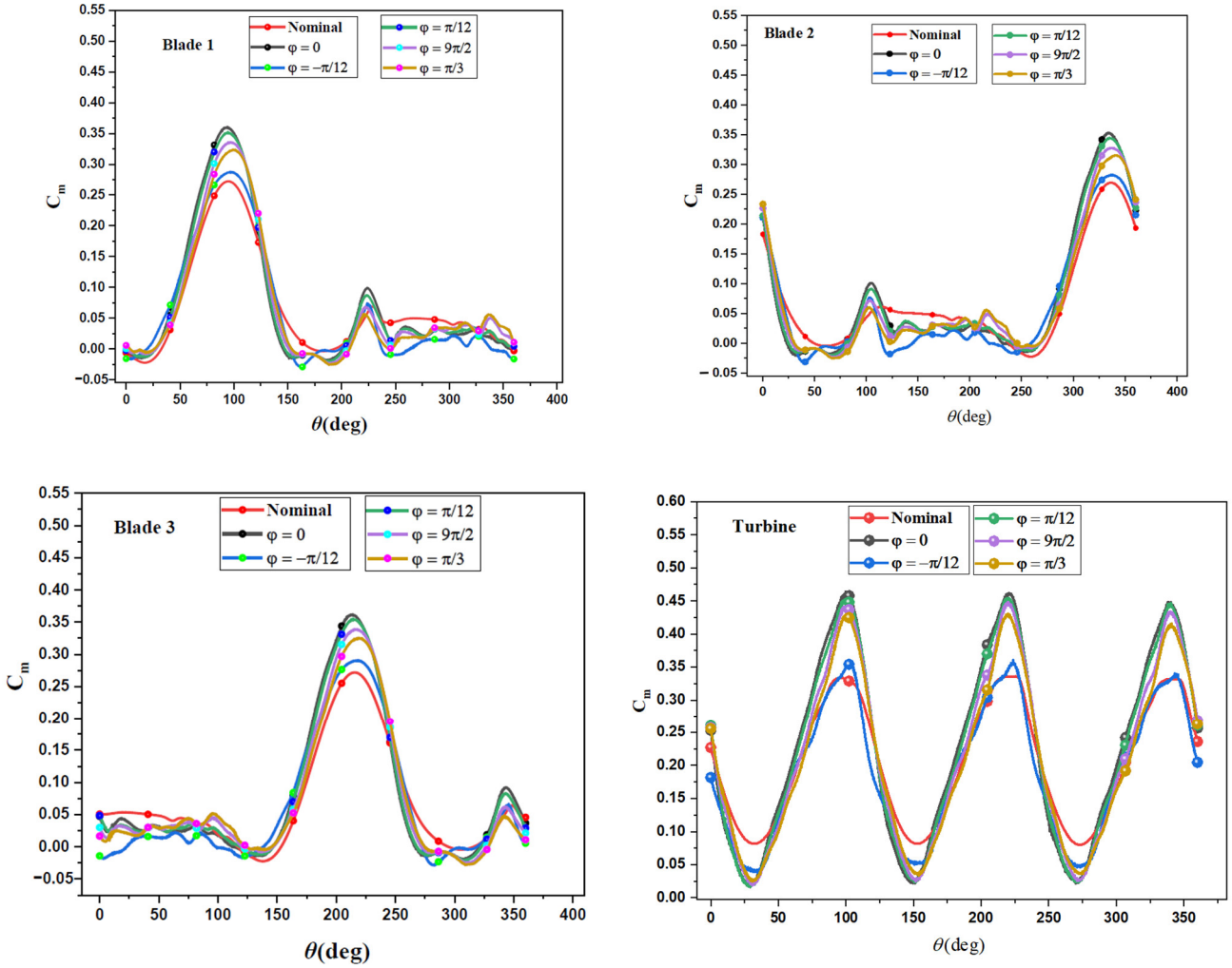


Figure 14. Effect of motion phase on the instantaneous individual and total torque coefficient (Cm).

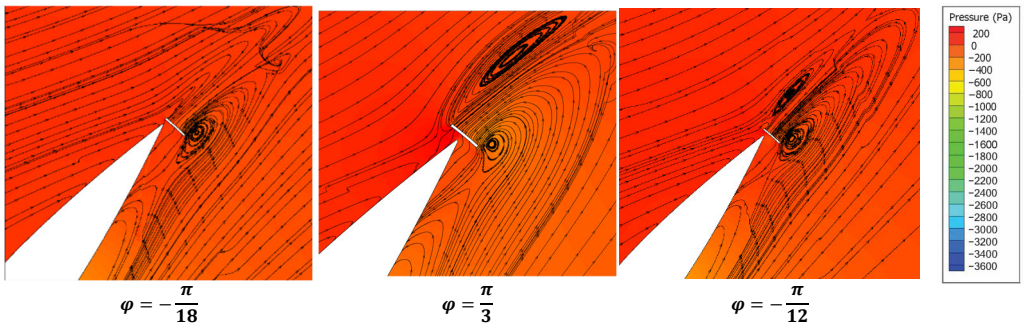
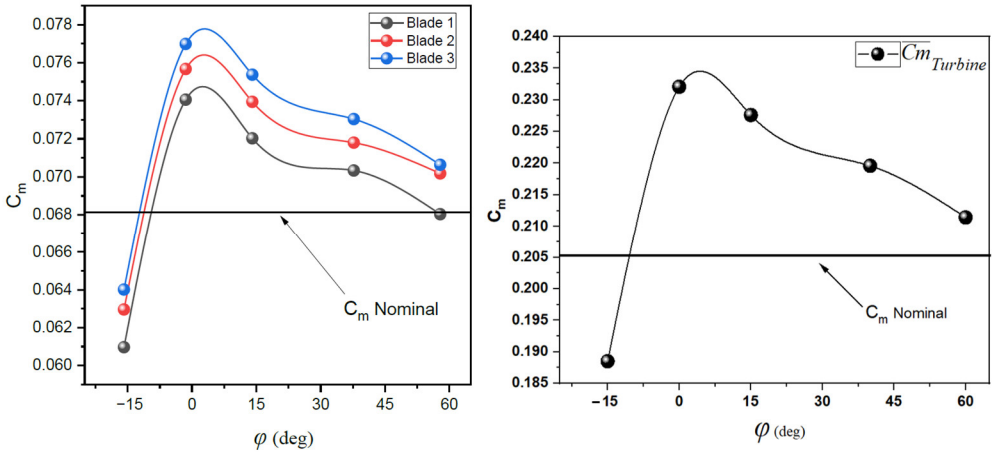


Figure 15. Effect of phase angle on the flow field and pressure distribution for θ = 45°.

The average torque coefficient (Cm) as function of phase angle is presented in Figure 16. The horizontal line represents Cm of nominal case. It was indicated that the average individual Cm decreases sharply with the increase in φ. This is attributed to the fact that at the first quarter of the turbine and by increasing φ, the length of OGF in the blade pressure side decreases, which decreases the size and the strength of the trailing edge vortex, and the airfoil loses energy to the surrounding fluid. It was indicated that for negative φ, the average Cm is less than that of the nominal case; this is because the OGF is fully located in the blade lower surface.



(**a**) (**b**)

Figure 16. Effect of motion phase on the average individual (**a**) and total (**b**) torque coefficient (Cm).

4.3. Effect of GF Length

In this section, the impact of the gurney flap's length on the effectiveness of energy extraction is investigated. Three lengths are used, which are L_1, L_2, and L_3. $L_1 = 2/3\ C \times \theta_1$, where θ_1 is the angle of swinging relative to the pitching center. Three swing angles are tested $\theta_1 = 1°, 2°$ and 3° (see Figure 17).

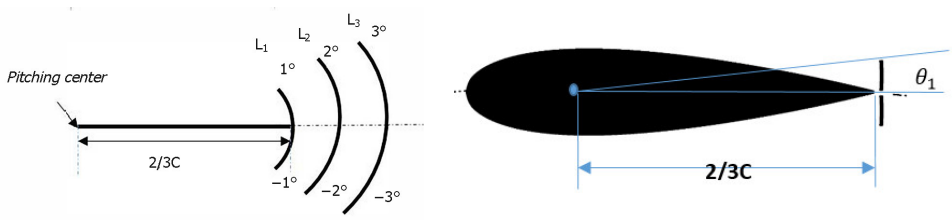


Figure 17. Selection method of GF length.

From Figure 18, it can be seen that the torque coefficient increases with the increase in the length of the swingable gurney flap under different flow conditions. Generally, by

increasing the length of the gurney flap, the boundary layer separates and consequently leads to the generation of trailing edge vortices [33]. Figure 19 indicates that the blade with the smallest OGF has a smooth fluid flow pattern near the trailing edge, which means there is less backflow, and its behavior is similar to that of a clean blade. The expansion of the GF length from L_1 to L_2 generates a larger trailing edge vortex.

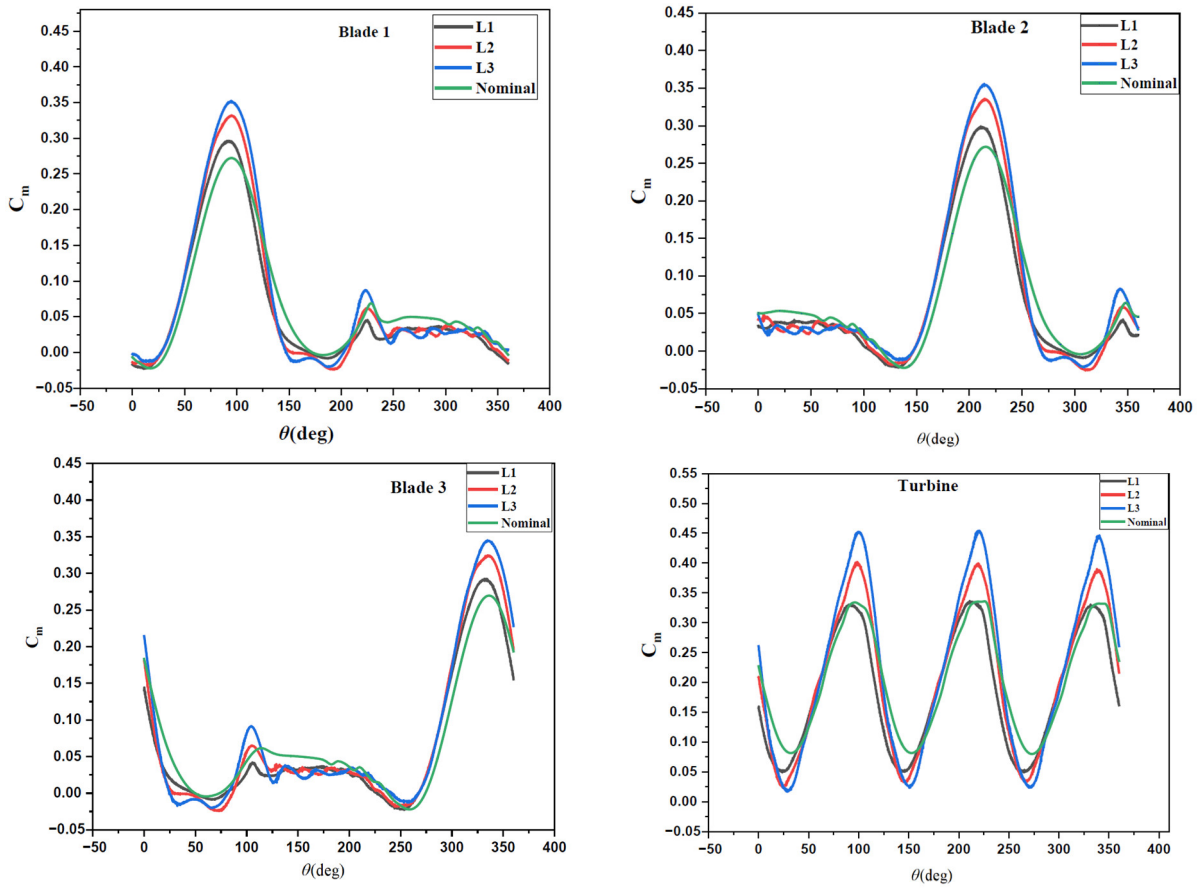


Figure 18. Effect of GF length on the instantaneous torque coefficient (Cm).

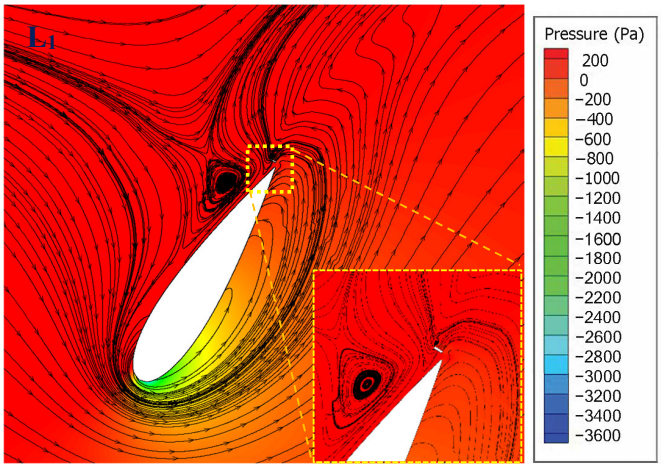


Figure 19. *Cont.*

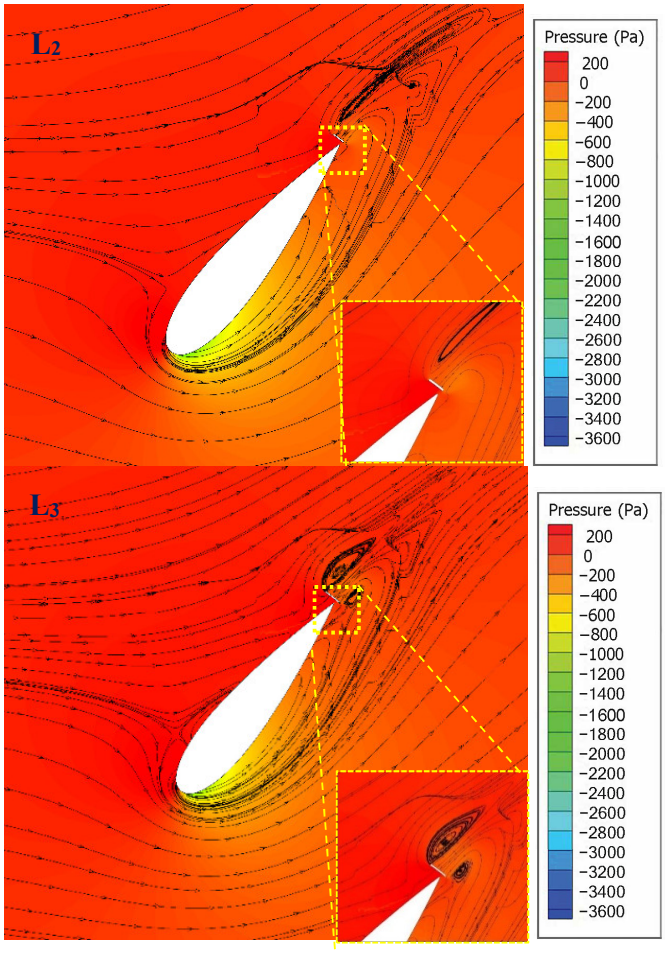


Figure 19. Comparison between flow field and pressure distribution.

In Figure 20, the depiction of the correlation between θ_1 and the average coefficient of movement can be observed. The evidence presented illustrates that as the angle θ_1 increases gradually, there is a significant increase in the power output obtained from the turbine. This finding highlights a clear positive relationship between θ_1 and the efficacy of the turbine in transforming kinetic energy from the airflow into useful mechanical power. These findings suggest that strategic manipulation of θ_1 could be pivotal in optimizing turbine performance.

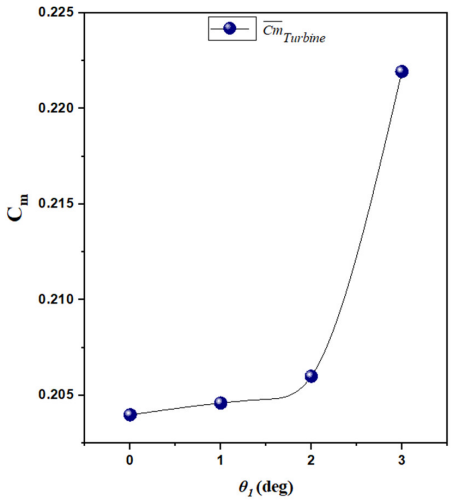


Figure 20. Effect of GF length on the average torque coefficient (Cm) for $\varphi = 0°$.

5. Conclusions

In this study, A CFD simulation is carried out to assess the effect of using an oscillating gurney flap OGF to improve the performance of Darrieus wind turbines. The OGF alters its position between the blade's upper and lower surfaces during the turbine's rotation. A two-dimensional (2D) numerical model is implemented using commercial code ANSYS-fluent 22.0. The equations of combined motion are applied through a user-defined function (UDF) and the overset dynamic mesh method is used. The findings of this work can be listed as follows:

- The good synchronization of the oscillating gurney flap motion with the blade motion enhances the lift force and the output power.
- The highest amount of energy is extracted in the first quarter of the turbine and the phase angle should be selected so that the OGF is fully located on the blade's upper surface.
- The Cm peak increases from 0.186 to 0.222 for all blades, which signifies an improvement of 19% in the average output power.

The proposed control method possesses the ability to rigidly change the shape of the blade with a simple movement of the gurney flap. So, it is applicable to both water and air turbines. Instead of using a fully deformable wing, we can achieve a similar result by using an oscillating gurney flap (modifying the airfoil camber). Regarding manufacturability, the proposed solution is easy to manufacture, as it requires a simple mechanism—like the windshield wiper engine—installed at the trailing edge to move the gurney flap.

Author Contributions: Conceptualization, A.Z. and N.L.; Methodology, N.L.; Software, A.Z. and M.T.B.; Validation, A.Z., S.L. and N.L.; Investigation, M.T.B. and N.L.; Resources, M.A. and N.L.; Writing—original draft, A.Z.; Writing—review & editing, A.Z., M.A., M.T.B., S.L. and N.L.; Visualization, M.A., S.L. and N.L.; Supervision, N.L.; Project administration, N.L. All authors have read and agreed to the published version of the manuscript.

Funding: This work has been supported by the EIPHI Graduate school (contract "ANR-17-EURE-0002") and by the Bourgogne-Franche-Comté Region.

Data Availability Statement: The original contributions presented in the study are included in the article, further inquiries can be directed to the corresponding author.

Conflicts of Interest: The authors declare no conflict of interest.

References

1. Olabi, A.G.; Obaideen, K.; Abdelkareem, M.A.; AlMallahi, M.N.; Shehata, N.; Alami, A.H.; Mdallal, A.; Hassan, A.A.M.; Sayed, E.T. Wind Energy Contribution to the Sustainable Development Goals: Case Study on London Array. *Sustainability* **2023**, *15*, 4641. [CrossRef]
2. Zereg, A.; Lebaal, N.; Aksas, M.; Derradji, B.; Chabani, I.; Mebarek-Oudina, F. CFD Analysis of a Vertical Axis Wind Turbine. In *Mathematical Modelling of Fluid Dynamics and Nanofluids*; CRC Press: Boca Raton, FL, USA, 2024; pp. 184–196.
3. Zhao, Z.; Wang, D.; Wang, T.; Shen, W.; Liu, H.; Chen, M. A review: Approaches for aerodynamic performance improvement of lift-type vertical axis wind turbine. *Sustain. Energy Technol. Assess.* **2022**, *49*, 101789. [CrossRef]
4. Zereg, A.; Bouzaher, M.T.; Aksas, M.; Lebaal, N. Performance enhancement of Savonius wind turbine through partially deformable blades. *Int. J. Simul. Multidiscip. Des. Optim.* **2024**, *15*, 8. [CrossRef]
5. Guo, J.; Zeng, P.; Lei, L. Performance of a straight-bladed vertical axis wind turbine with inclined pitch axes by wind tunnel experiments. *Energy* **2019**, *174*, 553–561. [CrossRef]
6. Zereg, A.; Lebaal, N.; Aksas, M.; Bassir, D. Numerical analysis and optimization of a vertical axis wind turbine with a flapped blade. In *AIP Conference Proceedings*; AIP Publishing: Melville, NY, USA, 2024; Volume 2989.
7. He, X.; Wang, J.J.; Yang, M.Q.; Ma, D.L.; Yan, C.; Liu, P.Q. Numerical simulation of gurney flaps lift-enhancement on a low reynolds number airfoil. *Sci. China Technol. Sci.* **2017**, *60*, 1548–1559. [CrossRef]
8. Arfaoui, B.; Bouzaher, M.T.; Guerira, B.; Bensaci, C.E. On the performance of swing arm flapping turbines. *J. Sol. Energy Eng. Trans. ASME* **2021**, 143. [CrossRef]
9. Jain, S.; Sitaram, N.; Krishnaswamy, S. Computational Investigations on the Effects of Gurney Flap on Airfoil Aerodynamics. *Int. Sch. Res. Not.* **2015**, *2015*, 402358. [CrossRef]
10. Aihara, A.; Mendoza, V.; Goude, A.; Bernhoff, H. Comparison of Three-Dimensional Numerical Methods for Modeling of Strut Effect on the Performance of a Vertical Axis Wind Turbine. *Energies* **2022**, *15*, 2361. [CrossRef]

11. Yang, J.; Yang, H.; Wang, X.; Li, N. Experimental Study of a Gurney Flap on a Pitching Wind Turbine Airfoil under Turbulent Flow Conditions. *J. Mar. Sci. Eng.* **2022**, *10*, 371. [CrossRef]
12. Ni, L.; Miao, W.; Li, C.; Liu, Q. Impacts of Gurney flap and solidity on the aerodynamic performance of vertical axis wind turbines in array configurations. *Energy* **2021**, *215*, 118915. [CrossRef]
13. Sun, G.; Wang, Y.; Xie, Y.; Lv, K.; Sheng, R. Research on the effect of a movable gurney flap on energy extraction of oscillating hydrofoil. *Energy* **2021**, *225*, 120206. [CrossRef]
14. Shubham, J.; Sitaram, N.; Krishnaswamy, S. Effect of Reynolds number on aerodynamics of airfoil with Gurney flap. *Int. J. Rotating Mach.* **2015**, *2015*, 628632.
15. Aubrun, S.; Leroy, A.; Devinant, P. A review of wind turbine-oriented active flow control strategies. *Exp. Fluids* **2017**, *58*, 134. [CrossRef]
16. Liebeck, R.H. Design of subsonic airfoils for high lift. *J. Aircr.* **1978**, *15*, 547–561. [CrossRef]
17. Gerontakos, P.; Lee, T. Dynamic stall flow control via a trailing-edge flap. *AIAA J.* **2006**, *44*, 469–480. [CrossRef]
18. Giguère, P.; Lemay, J.; Dumas, G. Gurney flap effects and scaling for low-speed airfoils. In Proceedings of the 13th Applied Aerodynamics Conference, San Diego, CA, USA, 19–22 June 1995; pp. 966–976. [CrossRef]
19. Pastrikakis, V.A.; Steijl, R.; Barakos, G.N.; Małecki, J. Computational aeroelastic analysis of a hovering W3 sokol blade with gurney flap. *J. Fluids Struct.* **2015**, *53*, 96–111. [CrossRef]
20. Bianchini, A.; Balduzzi, F.; Di Rosa, D.; Ferrara, G. On the use of Gurney Flaps for the aerodynamic performance augmentation of Darrieus wind turbines. *Energy Convers. Manag.* **2019**, *184*, 402–415. [CrossRef]
21. Xiao, Q.; Liu, W.; Incecik, A. Flow control for VATT by fixed and oscillating flap. *Renew. Energy* **2013**, *51*, 141–152. [CrossRef]
22. Feng, L.H.; Jukes, T.N.; Choi, K.S.; Wang, J.J. Flow control over a NACA 0012 airfoil using dielectric-barrier-discharge plasma actuator with a Gurney flap. *Exp. Fluids* **2012**, *52*, 1533–1546. [CrossRef]
23. Syawitri, T.P.; Yao, Y.; Yao, J.; Chandra, B. Geometry optimisation of vertical axis wind turbine with Gurney flap for performance enhancement at low, medium and high ranges of tip speed ratios. *Sustain. Energy Technol. Assess.* **2022**, *49*, 101779. [CrossRef]
24. Ismail, M.F.; Vijayaraghavan, K. The effects of aerofoil profile modification on a vertical axis wind turbine performance. *Energy* **2015**, *80*, 20–31. [CrossRef]
25. Chen, H.; Qin, N. Trailing-edge flow control for wind turbine performance and load control. *Renew. Energy* **2017**, *105*, 419–435. [CrossRef]
26. Mayda, E.A.; Van Dam, C.P.; Nakafuji, D.Y. Computational investigation of finite width microtabs for aerodynamic load control. In Proceedings of the 43rd AIAA Aerospace Sciences Meeting and Exhibit, Reno, Nevada, 10–13 January 2005; pp. 4541–4553.
27. Bouzaher, M.T.; Drias, N.; Guerira, B. Improvement of Energy Extraction Efficiency for Flapping Airfoils by Using Oscillating Gurney Flaps. *Arab. J. Sci. Eng.* **2019**, *44*, 809–819. [CrossRef]
28. Rezaeiha, A.; Montazeri, H.; Blocken, B. Characterization of aerodynamic performance of vertical axis wind turbines: Impact of operational parameters. *Energy Convers. Manag.* **2018**, *169*, 45–77. [CrossRef]
29. Zhu, H.; Hao, W.; Li, C.; Ding, Q. Numerical study of effect of solidity on vertical axis wind turbine with Gurney flap. *J. Wind Eng. Ind. Aerodyn.* **2019**, *186*, 17–31. [CrossRef]
30. Castelli, M.R.; Englaro, A.; Benini, E. The Darrieus wind turbine: Proposal for a new performance prediction model based on CFD. *Energy* **2011**, *36*, 4919–4934. [CrossRef]
31. Wang, Y.; Shen, S.; Li, G.; Huang, D.; Zheng, Z. Investigation on aerodynamic performance of vertical axis wind turbine with different series airfoil shapes. *Renew. Energy* **2018**, *126*, 801–818. [CrossRef]
32. Wang, B.; Zhu, B.; Zhang, W. New type of motion trajectory for increasing the power extraction efficiency of flapping wing devices. *Energy* **2019**, *189*, 116072. [CrossRef]
33. Zanotti, A.; Gibertini, G. Experimental assessment of an active L-shaped tab for dynamic stall control. *J. Fluids Struct.* **2018**, *77*, 151–169. [CrossRef]

Disclaimer/Publisher's Note: The statements, opinions and data contained in all publications are solely those of the individual author(s) and contributor(s) and not of MDPI and/or the editor(s). MDPI and/or the editor(s) disclaim responsibility for any injury to people or property resulting from any ideas, methods, instructions or products referred to in the content.